Soft Matter

Uncommon nonlinear rheological phenomenology in uniaxial extension of polystyrene solutions and melts

Journal:	*Soft Matter*
Manuscript ID	SM-ART-01-2020-000085.R1
Article Type:	Paper
Date Submitted by the Author:	13-Feb-2020
Complete List of Authors:	Yuan, Ruchao; Donghua University Liu, Jianning; University of Akron, Department of Polymer Science Wang, Yangyang; Oak Ridge National Laboratory Wang, Shi-Qing; University of Akron

Uncommon nonlinear rheological phenomenology in uniaxial extension of polystyrene solutions and melts

Ruchao Yuan[1,2], Jianning Liu[1], Yangyang Wang[3], and Shi-Qing Wang[1,*]

[1]Department of Polymer Science, University of Akron, Akron, Ohio 44325, United States

[2]College of Textiles, Donghua University, Shanghai 201620, China

[3]Center for Nanophase Materials Sciences, Oak Ridge National Laboratory

Oak Ridge, TN 37831

Abstract

This study examines nonlinear rheological responses to uniaxial extension of two entangled polystyrene (PS) solutions and two PS melts. Several unusual characteristics are revealed. The pair of the PS solutions have the same number of entanglements per chain (because of the same concentration) but the well separated effective glass transition temperatures T_g. When examined at a common effective rate of extension (e.g., the same Rouse-Weissenberg number Wi_R) and at a comparable distance from their respective T_g, the solution A with lower T_g, examined at the lower temperature, shows stronger stress responses when $Wi_R > 1$. At the same test temperature and a common Wi_R, the solution A is still found to display stronger stress response than the solution B that is made of the same fraction of parent PS in a second solvent also made of oligomeric PS of higher molecular weight. Finally, there are two features intrinsic to each of the four PS samples. First, at the same Wi_R they show reduced stress level at a lower temperature. Second, at sufficiently high applied Hencky rates, they show limiting rate behavior, i.e., undergoing the same melt rupture independent of the applied rate. These remarkable rheological responses indicate major theoretical difficulties facing the subject of nonlinear extensional rheology of entangled polymers.

* Corresponding author at swang@uakron.edu

I. Introduction

Among different types of soft matter materials, entangled polymers stand out as a most strongly viscoelastic and unique nonlinear in terms of their rheological responses. For example entangled melts and solutions can undergo considerable homogeneous extension, i.e., becoming many times longer than the initial length, without turning viscous or undergoing fracture. For practical purpose, e.g., a better understanding of industrial polymer processing, polymer entanglement dynamics has been extensively studied in the presence of strong deformation. However, after decades of research efforts, it has remained a challenge to make a satisfactory molecular-level quantification of how external deformation affects the entanglement network. Here the key questions are (a) where affine deformation originates from and (b) when affine like chain deformation ceases. Assumptions and simplifications made to address these two core questions, involving the Rouse chain retraction of the tube model[1, 2] and the recent idea of force imbalance,[3, 4] are both *ad hoc*. Schweizer and co-workers[5-12] have recently attempted to self-consistently treat chain uncrossability leading to entanglement in polymeric liquids using infinitely thin and rigid needles as an approximation of linear flexible chains and showed that entanglement constraint is of finite strength and can fail during or after large deformation upon force imbalance between interchain grip force and intrachain retractive force.

Nonlinear polymer rheology currently faces at least four analytical challenges that need to be addressed before the field can move forward. First, we need to have a realistic explanation of why entangled solutions and melts appear to show different rheological responses[13] when examined with filament stretching rheometry (FSR). Second, upon approaching the finite extensibility limit intrachain retractive forces acquire an enthalpic component[14] that has not been incorporated into the available theoretical modeling of entangled polymers. Third, no available theory can predict the melt rupture phenomenon[15] in fast stretching.[16] Here the scaling argument[4] based on the concept of intrachain entropic force fails, thus this difficulty is strongly related to the second challenge. Fourth, bead-spring-model based theoretical descriptions of nonlinear polymer rheology prescribe the same temperature dependence for the terminal relaxation time and segmental relaxation dynamics and consequently cannot predict when the time-temperature superposition principle fails to predict nonlinear rheological responses. To find solutions to these well-known difficulties, we need to accumulate more phenomenological information, which is the aim of the present work.

The first issue of steady-state viscosity increasing with the extensional rate in solutions and decreasing in melts[17-19] appears related to the question of whether steady-flow states of entangled solutions and melts can take place in globally homogeneous uniaxial extension. Such a discrepancy between solutions and melts is typically observed using FSR,[20] where the two ends of a filament under study are displaced in a manner that depends on actual rheological properties of the system. Specifically, a particular feedback mechanism is used to ensure that the middle of the filament is stretched at a fixed Hencky rate. Consequently the local strain at the middle of the specimen can deviate considerably from the nominal strain.[22] In other words, the middle exchanges dynamically with the rest of the filament and thus has a complicated boundary condition that is not predictable. As a consequence, through the feedback, various forms[21] of failure due the

tensile strain localization can be avoided. In absence of such an explicit rheological feedback, for example, when using Instron type[23-27] and Sentmanat extensional rheometry (SER),[28] entangled polymer melts have been observed to suffer various types (I to IV) of tensile strain localization,[21,29] and steady homogeneous flow could never be established even when the level of chain entanglement is very low (e.g., fewer than five entanglements per chain).[30] Thus, in the different regimes from I to IV as classified by Malkin and Petrie,[15] the feedbacks would be all different at different nominal Hencky rates,[22] due to the different types of tensile strain localization, except for melt rupture (regime IV). At sufficiently high rates where melt rupture takes place abruptly, FSR reports the same phenomenon as SER does because the rupture occurs instantly, too fast for the feedback mechanism to respond.

The second difficulty reveals the lack of more effective treatments of the relationship between chain conformational deformation and the corresponding intrachain forces.[1, 2, 4-12] Molecular models for chain dynamics from Rouse, reptation to the tube model of Doi-Edwards as well as the latest version of the tube theory have not incorporated the fact that upon approaching the finite extensibility limit the intrachain retractive force may involve enthalpic contributions. For a Gaussian chain, when chain's end-to-end distance R is $L = Nl_K$, the stretching force grows only linearly with extension to the limiting value of $f_0 = k_BT/l_K$. Given Kuhn length $l_K \sim 1$ nm for most linear flexible polymer chains, f_0 is merely a few pico-Newtons, which is far lower than revealed by experiment.[31] Well-known elastic models[31-35] such as the freely-jointed chain (FJC) model and wormlike-chain (WLC) model can prescribe arbitrarily high intrachain forces as a function of the end-to-end displacement and have been applied to fit the single-chain force measurements. The fitting has made researchers believe that intrachain forces as high as 100 pN can still be regarded to be entropic. Modified WLC models[36, 37], or extended FJC model[38] adds in an *ad hoc* manner a phenomenological term to account for the emergence of enthalpic chain tension. Unfortunately, such attempts to achieve a better fit with data does not answer when and how much enthalpic force shows up as a function of chain extension. It is encouraging that some theoretical attempts have been made to evaluate the chain tension in the limit of single chain[39-44] and explore how enthalpic forces arise. [45-49] Since the mesh size of the entanglement network in solutions can be significantly larger than that in melts, the finite chain extensibility limit is reached at lower stretching ratios in melts than in solutions. Consequently, the first issue is also tied to this second difficulty.

The stretching ratio to reach full extension on the Kuhn segment scale is given by $\lambda_0^* = (N_{e0})^{1/2}$ under the affine deformation condition where N_{e0} is the average number of Kuhn segments in an entanglement strand in pure melt. Similarly, the limiting stretching ratio is $\lambda^* = \lambda_0^* \phi^{-2/3}$ for an entangled solution with polymer concentration (volume fraction) ϕ because[50-52] $N_e = N_{e0}\phi^{-4/3}$. At any stage of extension characterized by the stretching ratio λ, the distance from the onset of non-Gaussian stretching and emergence of enthalpic tension may be characterized by the value of λ/λ_0^* and λ/λ^* respectively for melts and solutions. This ratio is smaller for the solution than for the melt by a factor of $\phi^{-2/3}$. This means that the intrachain retraction force would more gradually increase with the macroscopic strain λ in solutions than in melts. Consequently, a solution could be still undergoing Gaussian chain stretching while chains in an entangled melt already attains stronger retractive forces. Thus, it can be expected that in uniaxial extension the force imbalance

occurs at lower values of λ in melts than in solutions.[4] In other words, in entangled melts, we expect the yielding of the entanglement network to take place at a smaller Hencky strain than in entangled solutions. Consequently, the different responses of entangled solutions and melts can be alternatively accounted for without introducing the idea[18, 19] of differential segmental nematic interactions.

The striking phenomenon of melt rupture presents the third challenge: No quantitative argument is available to either predict or explain how entanglement locks up to act like chemical crosslinks at Hencky rates not much higher than the rate of Rouse relaxation. The intrachain force grows until a few chain scission events presumably lead to catastrophic force imbalance and collapse of the highly stretched entanglement network. Although it is conceptually clear that interchain uncrossability play an essential role to permit buildup of intrachain force to the magnitude of several nano-Newtons (necessary for bond breaking), we have no idea about how to model such topological excluded-volume constraints during fast extension. Apparently, at high enough rates the interchain uncrossability can be sufficiently effective to enable complete stretching until chain breaking. Such modeling has yet to be incorporated into the models for entangled polymer dynamics.

The fourth difficulty stems from the oversimplifications[4] made by all coarse-grained molecular models for chain dynamics. All theoretical descriptions assume the large-scale chain relaxation to have the same temperature dependence as the segmental dynamics controlling the localized interchain topological interactions that give rise to polymer entanglement. Since the segmental dynamics can have stronger temperature dependence than that of the overall chain dynamics,[53] the different temperature dependences have been reported[54] as indicating a failure of the time-temperature superposition principle (TTS). When such a difference does occur, nonlinear rheological responses may be expected to show temperature dependence that does not follow the William-Landel-Ferry (WLF) temperature shift, if the segmental dynamics prescribe the characteristics of the grip force.

This paper presents experimental results that have direct bearing on all of the four difficulties. Specifically, when SER is used to examine two polystyrene solutions of identical concentration and two PS melts of different molecular weights, different transient nonlinear rheological responses are observed at the same Weissenberg number *Wi* that is calculated according to the SAOS data. One type of the difference seems to originate from a key feature of the two PS solutions, each showing a breakdown of the TTS in the following sense: At the same *Wi* and different temperatures, the stress response to startup uniaxial extension is stronger at a lower temperature. Separately, PS melts are found to show the same melt rupture with identical stress vs. strain curves, independent of the applied rate. Furthermore, both PS melts and solutions can respectively show lower stress levels at lower temperatures at a given *Wi*. Finally, the PS solution involving oligomeric PS of higher molecular weight as the solvent is found to show weaker stress response at the same temperature and same *Wi*.

II. Experimental

A. Materials characterization

A.1 Molecular weight, its distribution and glass transition temperature

PS400K was synthesized at University of Akron, while PS900K and the oligomeric Polystyrene (oPS) PS1K (CAS#9003-53-6, CAT#578) were obtained from Pressure Chemical and Scientific Polymer Products, Inc, respectively. PS784K and the oPS PS3.5K were purchased from Polymer Source, Inc. PS784-1and PS784-3.5 were made with 52% of PS784K in 48 % of PS1K and 52% of PS784K in 48 % of PS3.5K, respectively. PS mixtures were prepared by first dissolving both PS784K and oPS in tetrahydrofuran (THF) to make solutions and adding 0.5% antioxidant (2,6 Di-tert-butyl-p-cresol) from Tokyo Chemical Industry CO., LTD with CAS# 128-37-0. Most of THF was evaporated slowly by placing the homogeneous solutions under a hood for several days, and the rest of THF was removed in a vacuum oven at an elevated temperature for 24 hours until the residual THF in the solution is undetectable.

Table 1 Molecular characterization of polystyrenes

Sample	M_w (kg/mol)	M_e (kg/mol)	Z	M_w/M_n	T_g (°C)	Source
PS784K	784	13	60	1.07	105	Polymer Source, Inc.
PS400K	409	13	31	1.01	105	Univ. of Akron
PS900K	900	13	69	1.06	105	Pressure Chemical
PS3.5K	3.5	N/A	N/A	1.05	61[55]	Polymer Source, Inc.
PS1K	1.1	N/A	N/A	1.12	29	Sci. Poly. Products, Inc.

The average molecular weights and molecular weight distributions MWD of various Polystyrenes are listed in Table 1, which also contains the information on the glass transition temperatures of these PS samples. Here the DSC traces of the two solutions were obtained using PerkinElmer DSC 4000 at a heating rate of 10 °C/min, as shown in Figure 1. Table 2 lists the values of T_g along with the number of entanglements per chain $Z = 784/13(0.52)^{-1.3} = 26$.

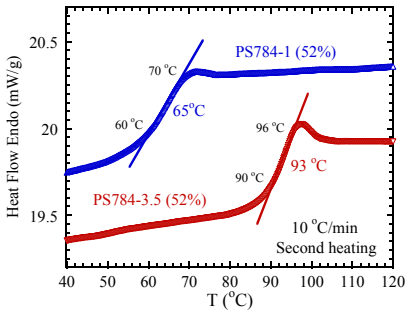

Fig. 1 Differential scanning calorimetric (DSC) measurements of PS784-3.5(52%) and PS784-1(52%).

Table 2 Molecular characterization of two polystyrene solutions

Sample	Components	ϕ	$M_e(\phi) = M_e(\phi)^{-1.3}$	Z	T_g (°C)
PS784-3.5 (52%)	784K + 3.5K	52% of 784K	30.4	26	93
PS784-1 (52%)	784K + 1K	52% of 784K	30.4	26	65

A.2 Linear viscoelastic characterization

Small amplitude oscillatory shear (SAOS) measurements of the storage and loss moduli G'

and G" were carried out as a function of frequency ω using an Advanced Rheometric Expansion System (ARES) rotational rheometer. In parallel plate geometry with diameter of 8 mm, the strain amplitude was chosen to be 5 % for temperatures well above T_g and 0.1 % for temperatures near T_g. From Fig. 2, we can extract the temperature dependence of the longest relaxation times τ_d of the two solutions, as shown in Table 3, where numbers in parentheses are read from the fitting curve in Fig. 3 below. These numbers allow us to compare the stress responses of the two solutions at the same applied value of *Wi*. Because melt rupture typically occurs at Hencky rates above the Rouse relaxation rate, it is instructive to characterize the rheological condition in terms of the Rouse-Weissenberg number Wi_R, defined as the product of Rouse relaxation time τ_R and Hencky rate $\dot{\varepsilon}$. It is common to use Osaki method[56] to evaluate τ_R in terms of the zero-rate viscosity η. However, when a reliable measurement of η is unavailable, use of the Osaki value of Rouse time could cause us to compare the two solutions *not* at the same Wi_R. For this reason, Wi_R is evaluated using the values of $\tau_R = \tau_d/3Z$, read from Table 1.

Table 3 Temperature dependence of terminal relaxation time τ_d (s) of two PS solutions

Sample	95 °C	100 °C	105 °C	110 °C	115 °C	120 °C	125 °C	130 °C	140 °C	150 °C	160 °C
PS784-1	53700	16300	5760	2290	(970)	437	(220)	113	33.5	12.7	5.4
PS784-3.5	/	/	/	897000	180000	47500	14500	5250	880	206	62.6

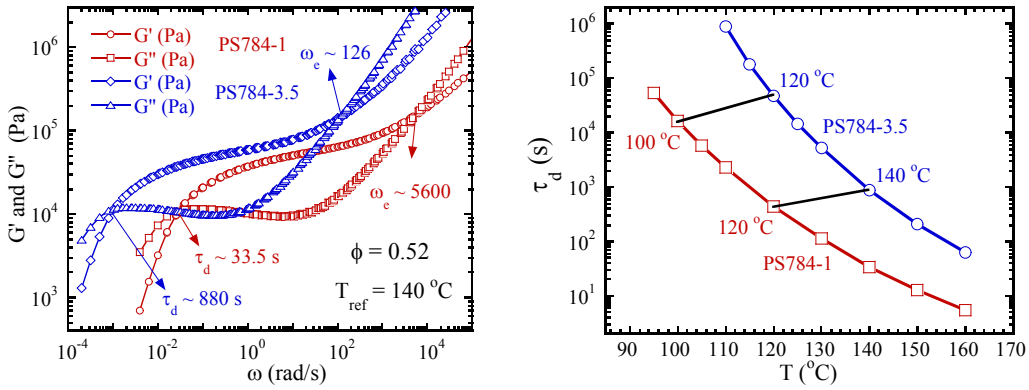

Fig. 2 Small-amplitude oscillatory shear measurements of the two solutions at reference temperature T_{ref} = 140 °C.

Fig. 3 WLF shift factor in terms of the terminal relaxation time τ_d, identified as the reciprocal crossover frequency (as indicated in Fig. 2). The two lines indicate the two pairs of test temperatures at which the two solutions have comparable values for τ_d.

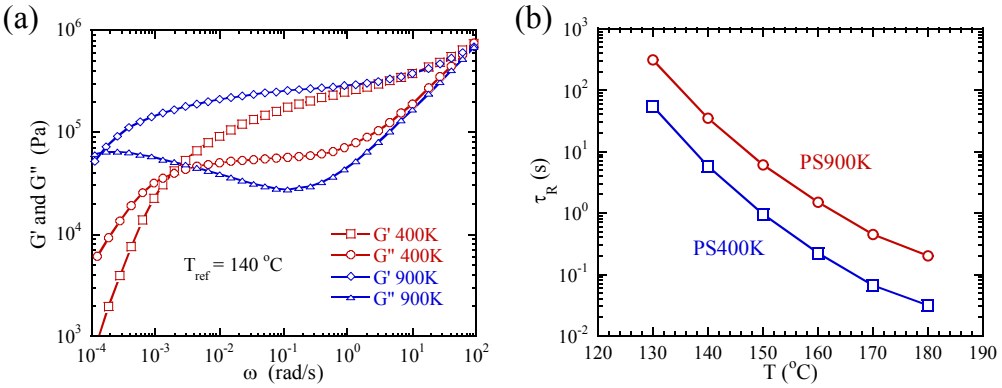

Figure 4 (a) Small-amplitude oscillatory shear measurements of PS400K and PS900K at reference temperature T_{ref} = 140 °C and (b) WLF shift factor in terms of the Rouse relaxation time τ_R, taken as $\tau_d/3Z$, with τ_d as the reciprocal crossover frequency and Z is either 31 or 69.

B. Experimental procedures

Stripe shaped samples were prepared by pressing PS solutions using a Carver press. A customized mold sandwiched by two Kapton polyimide film was employed with dimensions of 20 mm × 3 mm × 0.3 mm. Samples were first heated up to T_g + 70 °C. After equilibrium for 20 mins, a 5,000 lbs load was applied for 3 min then the load was released for 2 mins. More load was applied in the increment of 5,000 lbs load until reaching 20,000 lbs. Samples were equilibrated for 30 mins before taken out of the press to cool down to room temperature.

Uniaxial extension experiments were carried out using a first-generation SER fixture mounted on an ARES rotational rheometer (TA Instruments). The ARES oven was first heated to an elevated temperature (well above T_g). Then the stripe like sample was placed onto the hot surface of the two drums. A pre-tension was applied to stretch the sample to make it straight at an elevated temperature and then cooled down to the test temperature. ForPS784-3.5, the test temperatures were 120°C and 140 °C, while the extensional tests of PS784-1 were carried out at 95, 100 °C and 120 °C.

III. Results

According to the literature, entangled melts (rubbery polymers such as polyisoprene and styrene-butadiene rubber) display three types of filament breakup for Weissenberg number *Wi* > 1, categorized as regimes II, III and IV,[15] according to tensile decohesion, unstable necking and melt rupture respectively.[21] Even rather weakly entangled melt is capable of showing regime III and IV behavior.[30] Fig. 5 confirms that entangled molten thermoplastics such as PS900K behave in the same way. Moreover, PS solutions such as PS784-1 also exhibit necking and melt rupture behavior at two temperatures as shown in Fig. 6(a)-(b), with the solution PS784-3.5 showing the similar characteristics in Fig. 7(a)-(b). We note that the applied Hencky rates are generally still much lower than ω_e defined in Fig. 2. Below we analyze the temperature and rate dependences of the rheological behavior of the PS melts and solutions and compare their rheological characteristics. It is worth mentioning that homogenous uniaxial extension prevails in SER device well after the engineering stress maximum in regime III. Supporting information contains explicit video

verification to show that circles in Fig. 7(b) indeed show characteristics of regime III, with the sample staying uniform at least up to Hencky strain ε = 4.

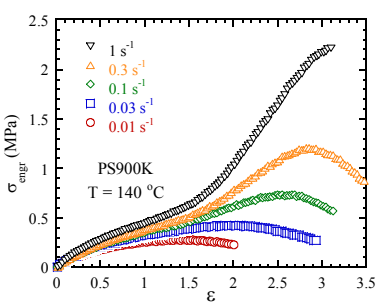

Fig. 5

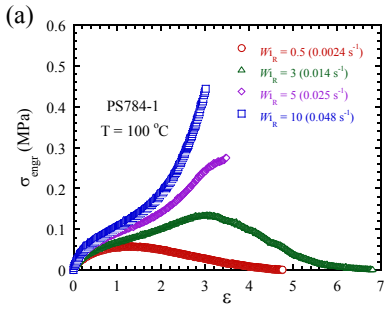

Fig. 6(a)

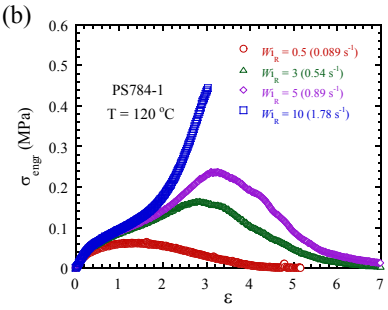

Fig. 6(b)

Fig. 5 Engineering stress vs. Hencky strain of PS900K at T = 140 °C under uniaxial extension, showing tensional decohesion (0.01 s^{-1}), necking (0.3 s^{-1}) and melt rupture (1 s^{-1}). Remove the symbols 3 to 20 s^{-1}

Fig. 6 Engineering stress vs. Hencky strain for PS784-1 under uniaxial extension at (a) T = 100 °C and (b) T = 120 °C for several values of Wi_R ranging from 0.5 to 10, showing melt rupture for Wi_R =5 and 10 at 100 °C and for Wi_R = 10 at 120 °C, where the numbers in the parentheses are the Hencky rate, a convention to follow for the rest of the figures.

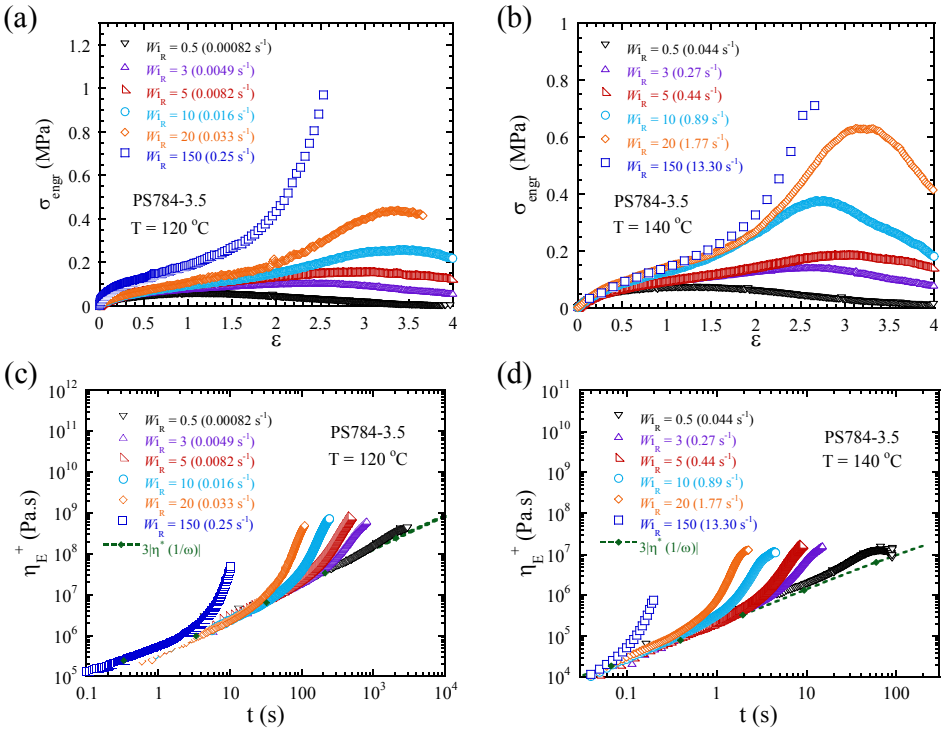

Fig. 7 Engineering stress vs. Hencky strain for PS784-3.5 under uniaxial extension at (a) T = 120 °C and (b) T = 140 °C for several values of Wi_R ranging from 0.5 to 150, showing melt rupture for Wi_R = 20 and 150 at 120 °C and for Wi_R =150 at 140 °C. (c) and (d) are the transient extensional viscosity based respectively on the data in (a) and (b).

A. Failure of time-temperature superposition (TTS)

A.1 Melt rupture at lower temperatures

The present PS solutions show a breakdown of the time-temperature superposition (TTS) when examined in terms of their nonlinear responses to uniaxial melt stretching. Specifically, at the same Rouse-Weissenberg number $Wi_R = \&\tau_R$, the test at lower temperature can produce melt rupture, i.e., regime IV behavior, whereas the same test at a higher temperature produces unstable necking (regime III). The stress vs. strain data at three temperatures are presented in Fig. 8. At $Wi_R = 5$ and T = 120 °C, PS784-1 solution shows a maximum in the engineering stress (circles) and eventually undergoes necking to terminate homogeneous melt extension. Here and hereafter we do not pinpoint the onset of necking because we focus on other rheological features in this study. At T = 100 °C, the same solution undergoes melt rupture instead as shown by the squares in Fig. 8. When the temperature is further decreased to 95 °C, even at a lower $Wi_R = 3.5$, melt rupture occurs instead of necking. Clearly, the nonlinear response to melt stretching no longer follows the temperature dependence prescribed by the SAOS measurements of the temperature dependence of the terminal relaxation time τ_d as presented in Fig. 3 by the squares. Such a type of breakdown of the TTS has been reported before.[57, 58] When the solvent has a considerably lower T_g than that of high molar-mass PS, as is the case for PS784-1, it is even possible for the failure of TTS to occur in strong startup shear.[59]

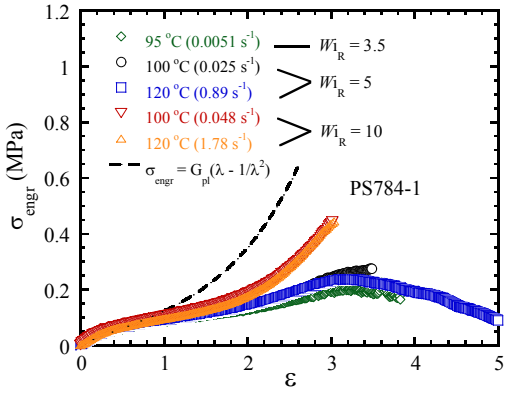

Fig. 8

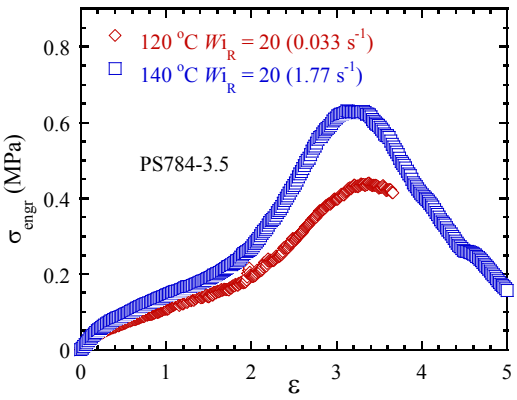

Fig. 9

Fig. 8 Engineering stress vs. Hencky strain for PS784-1 under uniaxial extension at various temperatures and three different effective rates given by Wi_R = 3.5, 5 and 10, showing necking (squares) and melt rupture (triangles, circles and diamonds). The dashed line shows the classical rubber elasticity formula as indicated in the figure where the plateau modulus $G_{pl} = G_N^0 \phi^{2.3} = 0.2 \times (0.52)^{2.3} = 0.044$ MPa.

Fig. 9 Engineering stress vs. Hencky strain for PS784-3.5 under uniaxial extension at various temperatures and three different effective rates given by Wi_R = 3.5, 5 and 10, showing necking (squares) and melt rupture (diamonds). A.2 Melt rupture at lower stress

There is an unusual feature in Fig. 8: The stress level associated with the melt rupture is lower at 95 °C than that involving necking at 120 °C, in contrast to the usual trend shown in Fig. 6(a)-(b) that melt rupture occurs at a higher stress level than that associated with the necking. This

character is not unique to PS784-1. We observe similar "stress reversal" in PS784-3.5. In other words, as shown in Fig. 9, PS784-3.5 shows a higher stress level at 140 °C (squares), associated with the yielding (signified the peak in σ_{engr}) and necking, and at 120 °C undergoes melt rupture at a lower stress level, both at the same applied $Wi_R = 20$. Since the two curves do not overlap in Fig. 9 and the melt rupture shows lower stress level, we can regard this feature as a different form of breakdown of the TTS from that demonstrated in the preceding section III.A.1.

A.3 Higher stress level at higher temperature

When PS784-1 and PS784-3.5 solutions are investigated at lower values of Wi_R, no melt rupture takes place. However, as shown in Fig. 10(a)-(b), the stress response is stronger at higher temperatures, unless either the applied rate is sufficiently low or the temperatures are sufficiently high, as indicated by the two sets of triangles in both figures. This trend also corroborates the findings presented in Fig. 8 and 9.

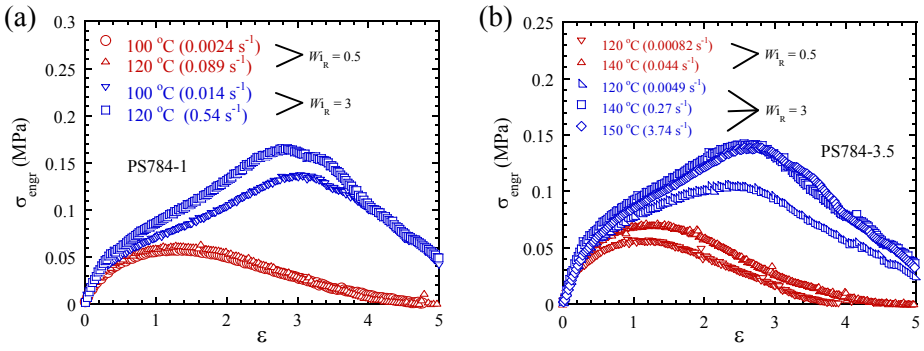

Fig. 10 Engineering stress vs. Hencky strain for (a) PS784-1 and (b) PS784-3.5 under uniaxial extension at various temperatures. In (a) the curves either overlap at $Wi_R = 0.5$ or at $Wi_R = 3$ higher stress level at 120 °C than at 100 °C. In (b), the curves at 140 and 150 °C overlap but stay higher than the curve at 120 °C; the two curves involving $Wi_R = 0.5$ show a smaller difference.

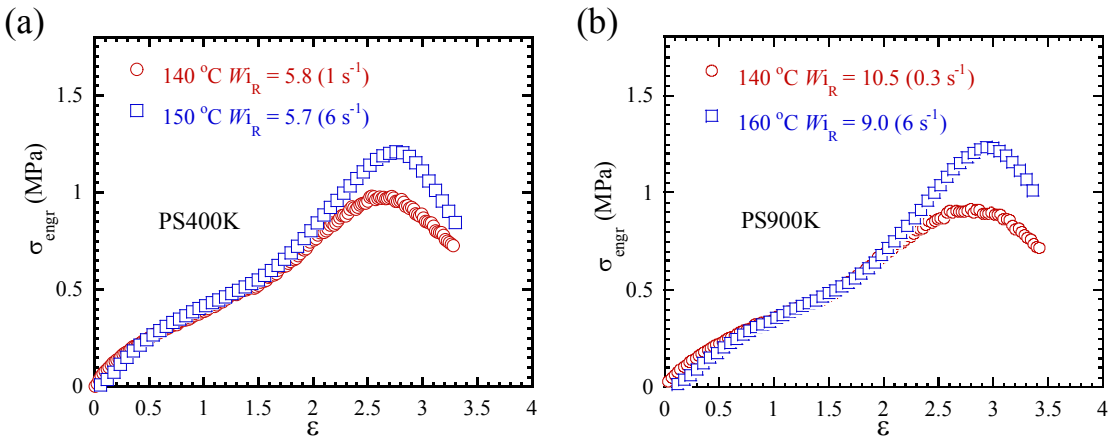

Fig. 11(a)-(b) Engineering stress vs. Hencky strain for (a) PS400K and (b) PS900K showing necking under uniaxial extension at two temperatures. The stress level is higher at 160 °C than at 140 °C although the tests were carried out at similar values of Wi_R.

Moreover, such unusual behavior is not unique to the two PS solutions. PS400K and PS900K also exhibit lower stress at the lower temperatures, as shown in Fig. 11(a) and 11(b) respectively. We will provide a speculative explanation in Discussion section IV.

B. Limiting rate behavior

It is noted from Fig. 8 that at Wi_R=10 the two curves overlapped, both showing melt rupture as if the TTS is recovered. Actually, this behavior may be related to some other feature rarely reported in the literature. We use PS400K and PS900K to illustrate the following new phenomenon of limiting rate. First of all, at a high rate corresponding to $Wi_R \sim 100$, PS400K, the TTS is also recovered as shown in Fig. 12. The origin of this agreement can be traced back to the fact that PS900K exhibits limiting rate behavior as shown in Fig. 13(a)-(b), i.e., all stress vs. strain curves converge to the same one, independent of the applied Hencky rates that are sufficiently high. Such lack of rate dependence of nonlinear melt rheology is previously unknown, to the best of our knowledge. It is also instructive to replot Fig. 13(b) in the conventional form of tensile stress growth coefficient η_E^+ vs. time, as shown in Fig. 13(c). We defer the implication/interpretation of this phenomenon to the Discussion section IV.

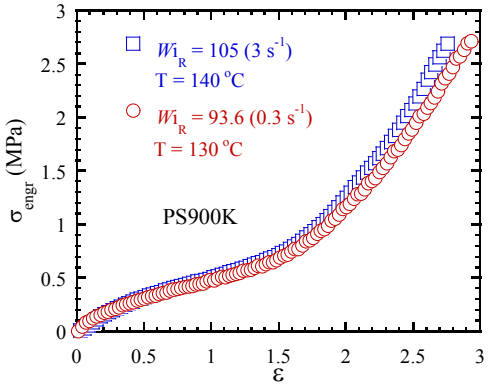

Fig. 12

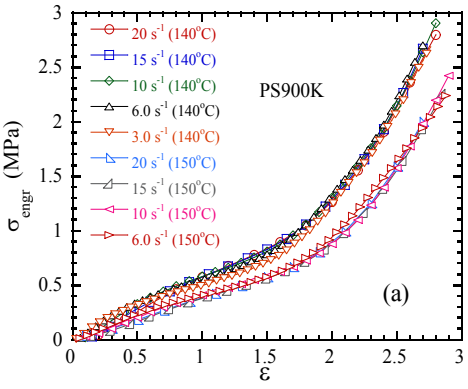

Fig. 13(a)

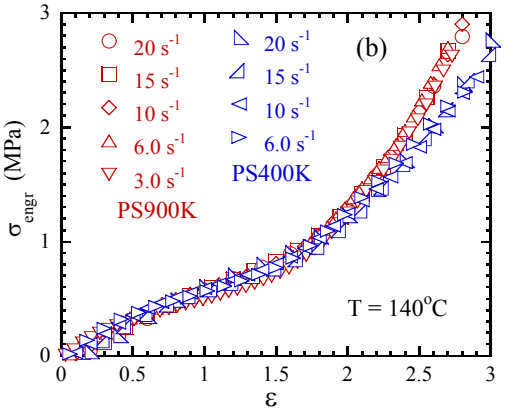

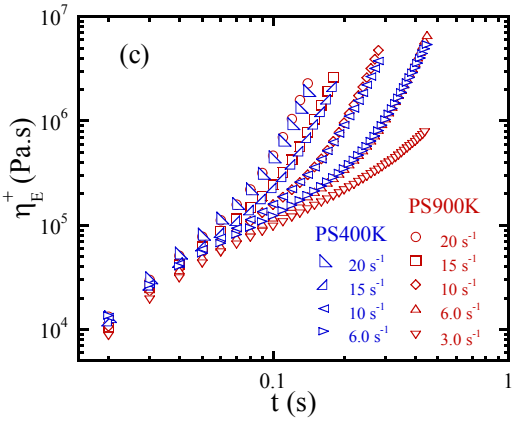

Fig. 13(b) Fig. 13(c)

Fig. 12 Engineering stress vs. Hencky strain for PS900K showing overlapping melt rupture behavior under uniaxial extension at two temperatures as if the TTS is recovered.

Fig. 13 Engineering stress vs. Hencky strain for (a) PS900K showing rate limiting behavior, i.e., identical melt rupture behavior independent of the applied rate at two different temperatures, (b) limiting rate behavior for PS400K and PS900K at 140 °C, (c) conventional plot of transient stress growth based on the data in (b).

C. Comparison at different temperatures: stronger stress response of PS784-1

Because of the strong plasticization effect, i.e., the considerably lower T_g of PS1K, when comparing PS784-1 solution with PS784-3.5 solution, the choice of lower test temperatures for PS784-1 as shown by the nearly horizontal lines in Fig. 3 is the condition that the experiments on the two solutions are done at comparable distances from T_g. Due to the self-concentration effect,[60] the parent PS chains in PS784-1 could show slower segmental dynamics, leading to high intermolecular grip force[59] and therefore stronger stress responses at the same Wi_R. This is plausible because we do not expect the self-concentration to affect the terminal chain dynamics revealed by the SAOS data. Fig. 14(a)-(b) indeed reveal remarkable contrasts between PS784-1 and PS784-3.5 at two pairs of temperatures (100, 120 °C) and (120, 140 °C) respectively. We see that at Wi_R = 10, PS784-1 shows melt rupture at both 100 and 120 °C whereas PS784-3.5 only displays yielding and necking, let alone at Wi_R = 5 because PS84-3.5 is investigated at the higher temperatures.

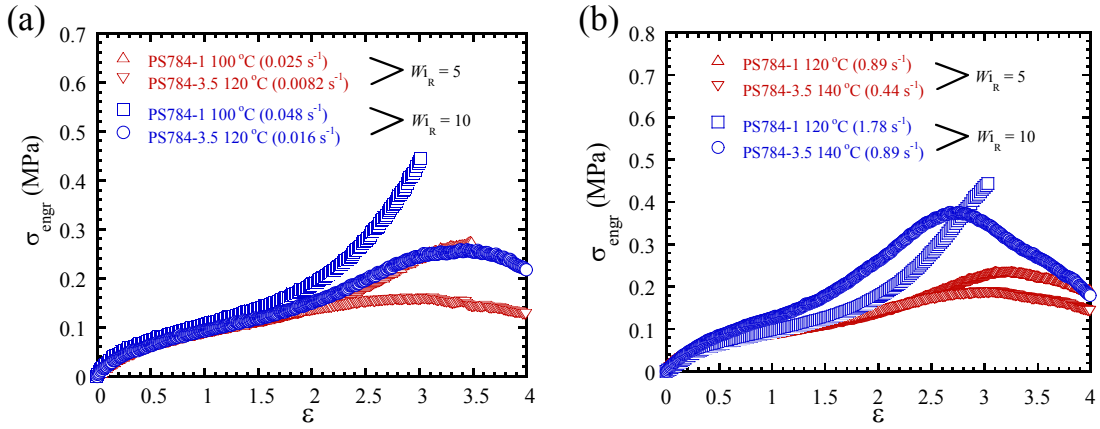

Fig. 14(a) Comparison between PS784-1 and PS784-3.5 in terms of engineering stress vs. Hencky strain from uniaxial extension at two pairs of temperature, (a) 100 and 120 °C and (b) 120 and 140 °C respectively, for Wi_R = 5 and 10.

D. Effect of solvent: different stress responses at same temperature and Wi_R

When comparing the two solutions, one additional contrast can be identified. Specifically, examined at the same temperature of 120 °C, PS784-1 still shows stronger response as shown in Fig. 15. At a common value of Wi_R = 10, PS784-1 shows melt-rupture whereas PS784-3.5 undergoes distinct necking. The difference between them remains also true at a lower Wi_R = 3 where both only undergo necking but exhibit different stress levels. Since the comparison involves

the same temperature, there must be a different reason to explain the stronger stress response of PS784-1 than the one that describes the contrast presented in III.C.

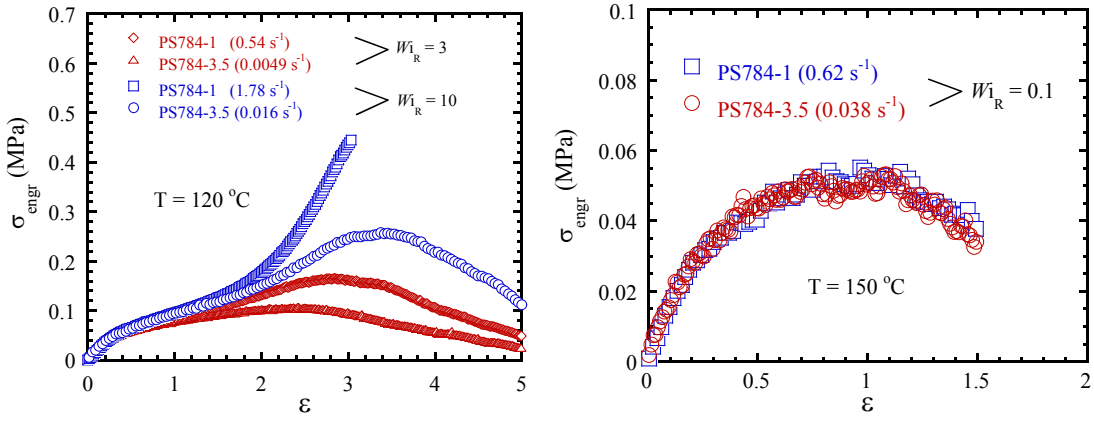

Fig. 15 Comparison between PS784-1 and PS784-3.5 in terms of engineering stress vs. Hencky strain from uniaxial extension at a common temperature of 120 °C for Wi_R = 3 and 10.

Fig. 16 Comparison between PS784-1 and PS784-3.5 in terms of engineering stress vs. Hencky strain from uniaxial extension at a common temperature of 150 °C for Wi_R = 0.1.

It is necessary to show that the difference disappears when the uniaxial extension involves a sufficiently low rate. Fig. 16 shows that at Wi_R = 0.1 the two solutions show identical responses at a common temperature of 150 °C.

IV. Discussions

There are four sets of phenomena, some of which involve both PS melts and its solutions and the rest are about the differences between the two PS solutions. Below we provide our specific interpretations. In the following discussion we will adopt the past interpretation[16] of the melt rupture behavior, i.e., regarding melt rupture to involve *entanglement lockup* and chain scission that unleashes a sharp network failure.

Regarding TTS: the temperature effects

According to Fig. 6(a)-(b), at a given temperature, melt rupture requires higher rates and shows higher stress than necking does. Fig. 8 (in III.A.1) reveals melt rupture at a lower temperature and necking at a higher temperature, which is a type of TTS breakdown similar to the one previously reported in the literature.[57, 58] This phenomenon suggests that at the same effective Hencky rate (i.e., the same value of Wi_R) the ability for the PS solutions to achieve entanglement lockup increases at a lower temperature where the parent PS chains can be expected to be more sluggish than revealed by the SAOS data. A similar explanation has been previously offered for analogous temperature effects on extensional rheology of entangled melts[57, 58] and shear rheology of PS solutions[59]. Since the nonlinear rheological responses are conceivably more sensitive to the segmental dynamics that have stronger temperature dependence than the terminal chain dynamics,[53] such a TTS failure can be expected. In other words, we propose that chain deformation is dictated by the interchain gripping, which depends on the local segmental

dynamics.[4] It is necessary to state that the segmental dynamics pertaining to the present cases have nothing in common with those encountered at much higher rates and lower temperatures[transient elasticity, Macromolecules 1992, 25, 3413-3415] where intersegmental interactions make a considerable contribution to the observed stress. In support of this statement, Fig. 8 shows that the stress response is below the classical rubber elasticity curve. In passing, we note that the TTS failure observed for linear viscoelastic responses,[54] can be argued to have the same origin: local dynamics exhibits stronger temperature dependence than the large-scale chain dynamics that involves spatial and temporal averaging.[53] A recent study[61] has further bearing on the matter of TTS failure.

Due to a combination of this temperature effect and the self-concentration effect, PS784-1 naturally displays stronger stress responses than PS784-3.5 at the same Wi_R that involves a similar level of Hencky rates, which are necessarily attained at different temperatures, i.e., lower testing temperature for PS784-1 than for PS784-3.5, 100 and 120 ^oC vs. 120 and 140 ^oC respectively, as shown in Fig. 14(a)-(b) in III.C.

There is another form of the TTS failure, previously unbeknown to us, which is presented in III.A.2-3. As a new temperature effect, both PS solutions show in Fig. 8 and 9 that the melt rupture (in diamonds) observed at lower temperatures showed a lower stress level than that exhibited by necking. This behavior plausibly indicates that partial force imbalance leading to loss of entanglement occurs more readily at a lower temperature, preventing the tensile stress from building up as much as it does at a higher temperature. The stress being lower at a lower temperature also takes place in regime III, as shown for the two PS solutions and two PS melts in Fig. 10(a)-(b) and 11(a)-(b). The earlier loss of entanglement due to the force imbalance suggests that there are higher intrachain retractive forces than there are interchain grip forces. This is possible, provided that there arise non-entropic intrachain forces. [14] Sufficiently high Wi_R and low temperature are the prerequisites. Indeed, the trend disappears at lower rates and higher temperatures, as noted in IIIA.3.

Limiting rate melt rupture

To the best of our knowledge, the limiting rate behavior shown in Fig. 13(a)-(b) has not been previously reported for non-associative polymer melts, except for an ionomeric PS based melt.[62] This phenomenon reveals a maximum fraction of entanglement that can lock up to result in melt rupture and therefore is directly associated with the structure of the chain network. In other words, the amount of entanglement lockup has an upper limit, accessible by application of a sufficiently high Hencky rate or Wi_R. It is not surprising that the limiting rate behavior as a reflection of the entanglement network structure is nearly molecular weight independent as shown by the near overlapping for all four rates in Fig. 13(c). On the other hand, the origin of the temperature dependence revealed in Fig. 13(a) remains unknown and unclear because there are at least two possibilities. Either the amount of chain tension for a given degree of chain stretching is different, e.g., higher at a lower temperature, or more entanglements lock up at a lower temperature to produce a higher stress level, or both factors contribute.

One more comment is in order regarding Fig. 13(b)-(c). The curves in Fig. 13(c), if interpreted conventionally, merely indicate different degrees of so called "strain hardening",† stronger at higher rates. The "rate dependence" in Fig. 13(c) is simply a demonstration that the upturn occurs earlier, i.e., at a shorter time but not at a higher strain for a higher rate. In other words, it would be difficult for us to tell from Fig. 13(c) that limiting-rate behavior, i.e., the rate independence (rather than rate dependence) as shown in Fig. 13(b) has occurred. Moreover, the lack of rate dependence can be regarded as another example of TTS breakdown.

Solvent molecular weight effect

The last but not least remarkable finding is that at the same Wi_R and same temperature PS784-1 still shows stronger stress responses as revealed in Fig. 15 in III.D. We propose the following speculative account. It is common knowledge that the terminal chain dynamics of an entangled solution depends on the solvent dynamics. With the solvent being a Rouse melt whose viscosity is linearly proportional to the chain length N_s of either PS1K or PS3.5K in the two solutions, it follows that apart from a complicated temperature dependence $f_1(T)$ or $f_{3.5}(T)$ that the solvent influences through its own T_g, the terminal time τ_d linearly varies with N_s, i.e., $\tau_d(T) = f_i(T)N_s$, where i = 1 or 3.5. At T=120 °C, the difference in τ_d between PS784-1 and PS784-3.5 in terms of the ratio $\tau_d(784\text{-}3.5)/\tau_d(784\text{-}1) = [f_{3.5}(T)/f_1(T)]Ns(PS3.5K)/Ns(PS1K) = 3.5[f_{3.5}(T)/f_1(T)]$ is 110 according to Fig. 3. Here the factor $\theta = [f_{3.5}(T)/f_1(T)] = 110/3.5 = 31$ is due to the large difference in T_g between PS3.5K and PS1K. In Fig. 15, the rheological characteristics of the two PS solutions are compared by applying a higher Hencky rate on PS784-1 by a factor 110 (instead of $\theta = 31$) than on PS784-3.5. If the magnitude of interchain grip force is not determined by having a common value of *Wi* for the two solutions, the applied Hencky rate to PS784-1 may be too high, as much as by a factor of 3.5. In other words, the higher stress shown by PS784-1 perhaps suggests that the magnitude of the grip force is not controlled by the terminal relaxation dynamics of the parent PS. In other words, when the two solutions are subjected to extensional deformation of the same Wi_R, as calculated based on the information from linear viscoelastic measurements, there is actually strong grip force available for PS783-1, resulting in the higher stress responses.

The concept of the grip force is applicable only for $Wi_R > 1$. The governing physics is different in regime II, e.g., at $Wi_R = 0.1$. In other words, at sufficiently low rates, the rheological response arises from the existence of an entropic cohesion barrier instead of the point-like interactions envisioned in terms of the grip force.[4] In this limit, the linear viscoelastic information from SAOS data provides a valid account of the polymer dynamics in the sense that the two PS solution can be expected to behave identically at a common value of $Wi_R << 1$. Fig. 16 indeed confirms that the difference between the two solutions vanishes when examined at $Wi_R = 0.1$.

V. Summary

In this study we have investigated two PS solutions and two PS melts to uncover several unusual characteristics associated with the nonlinear rheological responses to uniaxial extension at various temperatures that are not substantially above their glass transition temperatures. Apart from one characteristic of TTS breakdown similar to the previous reports to reveal melt rupture at

† For a detailed discussion of "strain hardening", see Chapter 8 in Ref. 4.

lower temperatures and only necking at higher temperatures, the other features seem previously unknown. (A) PS melts exhibits limiting rate behavior, showing identical melt rupture behavior at different applied rates. (B) Both PS solutions and melts show reduced stress levels at lower temperatures for the same effective Hencky rate, i.e., the same Wi_R. (C) At a common value of Wi_R PS784-1 solution shows stronger stress response than PS784-3.5 because the former is tested at a lower temperature. (D) Even at the same temperature PS784-1 is found to reveal stronger stress responses than PS874-3.5 for the same $Wi_R>1$, whereas identical rheological responses are observed for $Wi_R << 1$.

These previously unknown phenomena suggest that the subject of nonlinear extensional polymer rheology faces at least four difficulties outlined in the Introduction. The phenomenology appears far richer than the noted rheological differences between entangled melts and solutions[18, 19] and between two PS solutions[63] that are similar to behavior (C) listed above and studied in III.C. In case (C), the two PS solutions showed different responses because they were examined at different temperatures where the temperature dependence of segmental dynamics of parent PS chains is affected by the self-concentration effect in ways different from what is revealed by linear viscoelasticity.

This work is supported, in part, by NSF (DMR-0821697, DMR-1609977). Yuan acknowledge the financial support from China Scholarship Council.

References

1. M. Doi and S. F. Edwards, *The Theory of Polymer Dynamics*, Clarendon Press, Oxford, 1986.
2. R. S. Graham, A. E. Likhtman and T. C. B. McLeish, *J. Rheol.*, 2003, **47**, 1171-1200.
3. S. Q. Wang, S. Ravindranath, Y. Wang and P. Boukany, *J. Chem. Phys.*, 2007, **127**, 064903.
4. S.-Q. Wang, *Nonlinear Polymer Rheology: Macroscopic phenomenology and Molecular foundation*, Wiley, Hoboken, NJ, 2018.
5. D. M. Sussman and K. S. Schweizer, *Phys. Rev. Lett.*, 2011, **107**, 078102.
6. D. M. Sussman and K. S. Schweizer, *Phys. Rev. Lett.*, 2012, **109**, 168306.
7. D. M. Sussman and K. S. Schweizer, *Macromolecules*, 2012, **45**, 3270-3284.
8. D. M. Sussman and K. S. Schweizer, *Macromolecules*, 2013, **46**, 5684-5693.
9. D. M. Sussman and K. S. Schweizer, *J. Chem. Phys.*, 2013, **139**, 234904.
10. K. S. Schweizer and D. M. Sussman, *J. Chem. Phys.*, 2016, **145**, 214903.
11. S. J. Xie and K. S. Schweizer, *Macromolecules*, 2018, **51**, 4185-4200.
12. S. J. Xie and K. S. Schweizer, *Soft Matter*, 2018, **14**, 7052-7063.
13. Q. Huang, O. Mednova, H. K. Rasmussen, N. J. Alvarez, A. L. Skov, K. Almdal and O. Hassager, *Macromolecules*, 2013, **46**, 5026-5035.
14. Z. C. Zhao, X. Y. Zhao, J. N. Liu, W. Y. Wang, J. Mays and S. Q. Wang, *J. Chem. Phys.*, 2019, **151**, 13.
15. A. Y. Malkin and C. J. S. Petrie, *J. Rheol.*, 1997, **41**, 1-25.
16. P. P. Lin, J. N. Liu, Z. C. Zhao, Z. G. Wang and S. Q. Wang, *Polymer*, 2017, **124**, 68-77.
17. Q. Huang, L. Hengeller, N. J. Alvarez and O. Hassager, *Macromolecules*, 2015, **48**, 4158-4163.
18. T. Yaoita, T. Isaki, Y. Masubuchi, H. Watanabe, G. Ianniruberto and G. Marrucci, *Macromolecules*, 2012, **45**, 2773-2782.
19. G. Ianniruberto, A. Brasiello and G. Marrucci, *Macromolecules*, 2012, **45**, 8058-8066.
20. G. H. McKinley and T. Sridhar, *Annu. Rev. Flu. Mech.*, 2002, **34**, 375-415.
21. X. Zhu and S.-Q. Wang, *J. Rheol.*, 2013, **57**, 223-248.
22. J. M. R. Marín, J. K. Huusom, N. J. Alvarez, Q. Huang, H. K. Rasmussen, A. Bach, A. L. Skov and O. Hassager, *J. Non-Newton. Fluid*, 2013, **194**, 14-22.
23. G. Vinogradov, *Rheol. Acta*, 1975, **14**, 942-954.
24. E. Kamei and S. Onogi, 1975.
25. Y. Ide and J. L. White, *J. Non-Newton. Fluid*, 1977, **2**, 281-298.
26. G. Vinogradov, V. Dreval, E. Borisenkova, M. Kurbanaliev and V. Shalganova, *Rheol. Acta*, 1981, **20**, 433-442.
27. A. Y. Malkin and G. V. Vinogradov, *Vysokomolekulyarnye Soedineniya Seriya A*, 1985, **27**, 227-237.
28. M. L. Sentmanat, *Rheol. Acta*, 2004, **43**, 657-669.
29. A. Y. Malkin and C. Petrie, *J. Rheol. (1978-present)*, 1997, **41**, 1-25.
30. Y. Feng, J. Liu, S.-Q. Wang, K. Ntetsikas, A. Avgeropoulos, M. Kostas and J. Mays, *Journal of Rheology*, 2019, **63**, 763-771.
31. M. Rief, F. Oesterhelt, B. Heymann and H. E. Gaub, *Science*, 1997, **275**, 1295-1297.
32. A. Janshoff, M. Neitzert, Y. Oberdörfer and H. Fuchs, *Angewandte Chemie International Edition*, 2000, **39**, 3212-3237.
33. M. I. Giannotti and G. J. Vancso, *ChemPhysChem*, 2007, **8**, 2290-2307.
34. M. Rief, J. M. Fernandez and H. E. Gaub, *Phys. Rev. Lett.*, 1998, **81**, 4764.
35. S. B. Smith, Y. Cui and C. Bustamante, *Science*, 1996, **271**, 795-799.
36. J. F. Marko and E. D. Siggia, *Macromolecules*, 1995, **28**, 8759-8770.
37. T. Odijk, *Macromolecules*, 1995, **28**, 7016-7018.
38. B. Zhang and J. S. Evans, *Biophys. J.*, 2001, **80**, 597-605.
39. H. J. Kreuzer, R. L. Wang and M. Grunze, *New J. Phys.*, 1999, **1**, 21.
40. H. Kreuzer and M. Grunze, *EPL (Europhysics Letters)*, 2001, **55**, 640.

41. H. Kreuzer, S. Payne and L. Livadaru, *Biophysical journal*, 2001, **80**, 2505-2514.
42. L. Livadaru, R. Netz and H. Kreuzer, *The Journal of chemical physics*, 2003, **118**, 1404-1416.
43. F. Hanke and H. Kreuzer, *Eur. Phys. J. E*, 2007, **22**, 163-169.
44. F. Hanke and H. Jürgen Kreuzer, *Biointerphases*, 2006, **1**, 11-17.
45. H. Wei and T. G. van de Ven, *Applied Spectroscopy Reviews*, 2008, **43**, 111-133.
46. F. Oesterhelt, M. Rief and H. E. Gaub, *New J. Phys.*, 1999, **1**, 11.
47. D. E. Hanson and R. L. Martin, *J. Chem. Phys.*, 2009, **130**, 6.
48. T. Hugel and M. Seitz, *Macromol. Rapid Commun.*, 2001, **22**, 989-1016.
49. D. E. Hanson and J. L. Barber, *Contemp. Phys.*, 2015, **56**, 319-337.
50. R. H. Colby, L. J. Fetters, W. G. Funk and W. W. Graessley, *Macromolecules*, 1991, **24**, 3873-3882.
51. R. H. Colby and M. Rubinstein, *Macromolecules*, 1990, **23**, 2753-2757.
52. S. Wang, S.-Q. Wang, A. Halasa and W.-L. Hsu, *Macromolecules*, 2003, **36**, 5355-5371.
53. A. P. Sokolov and K. S. Schweizer, *Phys. Rev. Lett.*, 2009, **102**, 248301.
54. D. J. Plazek, *Journal of rheology*, 1996, **40**, 987-1014.
55. J. Erichsen, T. Shiferaw, V. Zaporojtchenko and F. Faupel, *The European Physical Journal E*, 2007, **24**, 243-246.
56. K. Osaki, T. Inoue, T. Uematsu and Y. Yamashita, *J. Polym. Sci., Part B: Polym. Phys.*, 2001, **39**, 1704-1712.
57. H. Sun, K. Ntetsikas, A. Avgeropoulos and S.-Q. Wang, *Macromolecules*, 2013, **46**, 4151-4159.
58. P. Lin, J. Liu, Z. Zhao, Z.-G. Wang and S.-Q. Wang, *Polymer*, 2017, **124**, 68-77.
59. G. Liu and S.-Q. Wang, *Macromolecules*, 2016, **49**, 9647-9654.
60. T. P. Lodge and T. C. McLeish, *Macromolecules*, 2000, **33**, 5278-5284.
61. T. Shahid, C. Clasen, F. Oosterlinck and E. van Ruymbeke, *Macromolecules*, 2019, **52**, 2521-2530.
62. A. Shabbir, Q. Huang, G. P. Baeza, D. Vlassopoulos, Q. Chen, R. H. Colby, N. J. Alvarez and O. Hassager, *J. Rheol.*, 2017, **61**, 1279-1289.
63. Q. Huang, N. J. Alvarez, Y. Matsumiya, H. K. Rasmussen, H. Watanabe and O. Hassager, *ACS Macro Lett.*, 2013, **2**, 741-744.

Table of Content

Unusual nonlinear rheological phenomenology in uniaxial extension of polystyrene solutions and melts

Ruchao Yuan, Jianning Liu, Yangyang Wang, and Shi-Qing Wang